Catalysis Today 145 (2009) 188–194

Contents lists available at ScienceDirect

Catalysis Today

journal homepage: www.elsevier.com/locate/cattod

In-situ characterization of water–gas shift catalysts using time-resolved X-ray diffraction

José A. Rodriguez [a,*], Jonathan C. Hanson [a], Wen Wen [a], Xianqin Wang [a], Joaquín L. Brito [b], Arturo Martínez-Arias [c], Marcos Fernández-García [c]

[a] *Chemistry Department, Brookhaven National Laboratory, Upton, NY 11973, USA*
[b] *Instituto Venezolano de Investigaciones Cientificas, Apdo. 20632, Caracas 1020-A, Venezuela*
[c] *Instituto de Catálisis y Petroleoquímica, Centro Superior de Investigaciones Cientificas, Campus Cantoblanco, 28049 Madrid, Spain*

ARTICLE INFO

Article history:
Available online 8 January 2009

Keywords:
X-ray diffraction
In-situ characterization
Water–gas shift reaction
Hydrogen production

ABSTRACT

Time-resolved X-ray diffraction (XRD) has emerged as a powerful technique for studying the behavior of heterogeneous catalysts (metal oxides, sulfides, carbides, phosphides, zeolites, etc.) *in-situ* during reaction conditions. The technique can identify the active phase of a heterogeneous catalyst and how its structure changes after interacting with the reactants and products (80 K < T < 1200 K; P < 50 atm). In this article, we review a series of recent works that use *in-situ* time-resolved XRD for studying the water–gas shift reaction (WGS, $CO + H_2O \rightarrow H_2 + CO_2$) over several mixed-metal oxides: $CuMoO_4$, $NiMoO_4$, $Ce_{1-x}Cu_xO_{2-\delta}$ and $CuFe_2O_4$. Under reaction conditions the oxides undergo partial reduction. Neutral Cu^0 (i.e. no Cu^{1+} or Cu^{2+} cations) and Ni^0 are the active species in the catalysts, but interactions with the oxide support are necessary in order to obtain high catalytic activity. These studies illustrate the important role played by O vacancies in the mechanism for the WGS. In the case of $Ce_{1-x}Cu_xO_{2-\delta}$, Rietveld refinement shows expansions/contractions in the oxide lattice which track steps within the WGS process: $CO(gas) + O(oxi) \rightarrow CO_2(gas) + O(vac)$; $H_2O(gas) + O(vac) \rightarrow O(oxi) + H_2(gas)$.

1. Introduction

The development of techniques for characterizing the structural properties of catalysts under the high-pressure conditions of industrial processes is widely recognized as a top priority in the area of heterogeneous catalysis. Under reaction conditions a catalyst can undergo chemical transformations that drastically modify its composition with respect to that obtained during the synthesis of the material. To optimize the performance of the catalyst, it is desirable to know what is its active phase. Investigations at Brookhaven National Laboratory have established the feasibility of conducting sub-minute, time-resolved *in-situ* X-ray diffraction (XRD) experiments under a wide variety of temperature and pressure conditions (80 K < T < 1200 K; P < 50 atm) [1]. This important advance results from combining the high intensity of synchrotron radiation with new parallel data-collection devices [1]. Similar *in-situ* diffraction facilities have also been established at the Daresbury synchrotron [2] and HASYLAB [3]. Using time-resolved XRD, one can get information about [1]:

- Phase identification and composition of catalysts under reaction conditions.
- Kinetics of crystallization of bulk solids and nanoparticles.
- Crystallite size as a function of time/temperature.
- Identify crystalline or amorphous intermediates during phase transitions occurring in bulk solids or nanoparticles.
- Real-time crystal structure refinement.

Examples of problems studied to date with time-resolved XRD and related to catalysis include [1,4–11]:

- Hydrothermal synthesis of zeolites.
- Hydrothermal conversion of zeolites.
- Binding of substrates and inhibitors in zeolites.
- Reduction/oxidation cycles in oxide catalysts.
- Phase transformations in oxide catalysts under reaction conditions (for example, the partial oxidation of hydrocarbons and the water–gas shift reaction).
- Sulfidation of oxide precursors for HDS catalysts.
- Regeneration of S-poisoned oxide catalysts.
- Synthesis of metal phosphide catalysts.

An early review article by Norby and Hanson [1] was focused on the applications of the technique in solid-state chemistry and materials science. In this article, we review a series of recent works

* Corresponding author. Tel.: +1 631 344 2246; fax: +1 631 344 5815.
E-mail address: rodrigez@bnl.gov (J.A. Rodriguez).

0920-5861/$ – see front matter © 2008 Elsevier B.V. All rights reserved.
doi:10.1016/j.cattod.2008.11.018

that use *in-situ* time-resolved XRD for studying the water–gas shift reaction (WGS, $CO + H_2O \rightarrow H_2 + CO_2$) over several mixed-metal oxides: $CuMoO_4$ [9], $NiMoO_4$ [10], $Ce_{1-x}Cu_xO_{2-\delta}$ [11] and $CuFe_2O_4$. *In-situ* XRD has also been previously used to study the WGS on CuO-ZnO catalysts [3]. At present, nearly 95% of the hydrogen supply is produced from the reforming of crude oil, coal, natural gas, wood, organic wastes and biomass. The reformed fuel contains 1–10% CO, which degrades the performance of the Pt electrode in fuel cell systems. In order to get clean hydrogen for fuel cells and other industrial applications, the WGS and CO oxidation ($2CO + O_2 \rightarrow 2CO_2$) processes are critical [12]. Fe–Cr and Cu–Zn oxides are the commercially used catalysts for the WGS at temperatures between 350–500 and 180–250 °C, respectively. However, these oxide catalysts are pyrophoric and normally require lengthy and complex activation steps before usage [12]. Consequently other catalysts are being sought. Several mixed-metal oxides have been tested as catalyst precursors for the water–gas shift [9–12]. In principle, the combination of two metals in an oxide matrix can produce materials with novel chemical and physical properties that can lead to a superior performance in technological applications. Recent studies indicate that catalysts which combine copper with ceria or molybdena have a higher activity for the WGS than the conventional combination of copper and zinc oxide [13]. There is no general agreement about the oxidation state of copper in these catalysts, with Cu^{2+}, Cu^{1+} and Cu^0 being proposed as the active species [3,12,13]. In order to address this issue, *in-situ* characterization of the WGS catalysts is necessary.

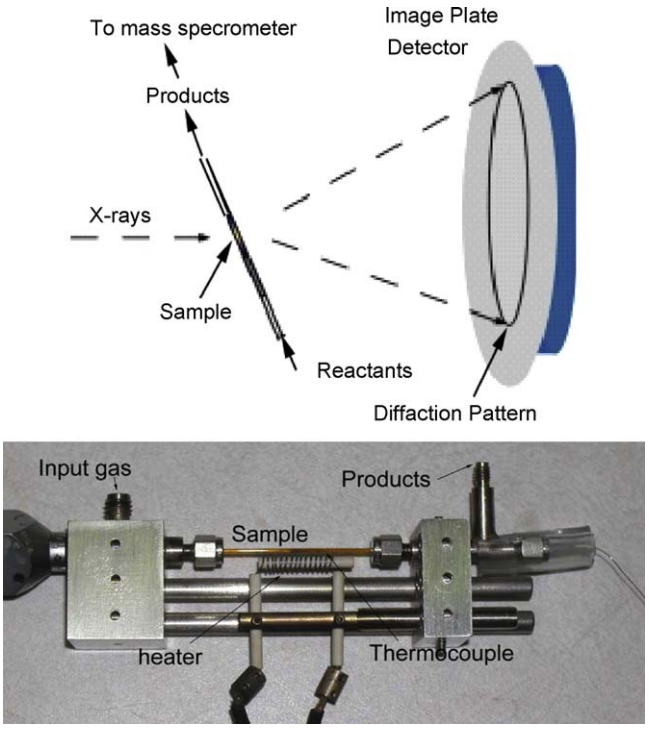

Fig. 1. Scheme of experimental set-up (top) and sapphire flow cell (bottom) for *in-situ* time-resolved X-ray diffraction studies of catalysts.

2. Experimental

In previous works, time-resolved XRD was used to characterize the structural behavior of CuO–ZnO [3], $CuMoO_4$ [9], $NiMoO_4$ [10], and $Ce_{1-x}Cu_xO_{2-\delta}$ [11] under WGS reaction conditions. In this article we present, for the first time, similar studies for $CuFe_2O_4$. The time-resolved diffraction data were collected on beam line X7B of the National Synchrotron Light Source (NSLS) [1]. The oxide samples (1–2 mg) were loaded into a sapphire capillary (micro-reactor) that was attached to a flow system (see Fig. 1) [14,15]. A small resistance heater could be set around or near the capillary, and the temperature was monitored with a 0.1 mm chromel-alumel thermocouple that was placed inside the capillary near the sample. The WGS reaction was carried out isothermally at 350, 400 and 500 °C, with a flow of 5% CO/He gas mixture through a water bubbler at a rate of ~10 mL/min. The exit of the micro-reactor was near ambient pressure. The composition of the gas leaving the capillary could be determined by means of gas chromatography and/or mass spectrometry. A MAR345 detector was used to record full X-ray patterns (see Fig. 1) and the powder rings were first integrated with the FIT2D code [16]. The FIT2D parameters for the integration of the data were obtained with a standard LaB_6 crystal compound. From the XRD data, occupancies of atoms, accurate lattice constants, and the concentration of phases appearing during reaction were determined by a Rietveld analysis using the GSAS (general structure analysis system) program [17].

3. Results and discussion

3.1. Water–gas shift reaction on $CuMoO_4$ and β-$NiMoO_4$

$CuMoO_4$ and β-$NiMoO_4$ have been tested as catalysts or catalyst precursors for the WGS reaction [9,10]. These mixed-metal oxides have a crystal structure in which cations of Mo and Cu or Ni alternate, see Fig. 2. $CuMoO_4$ and β-$NiMoO_4$ are interesting as catalyst precursors because they contain a well-defined atomic ratio of Cu:Mo or Ni:Mo. Fig. 3(a) displays *in-situ* XRD patterns collected during the water–gas shift reaction process on β-$NiMoO_4$ [10]. The β-$NiMoO_4$ sample remained unchanged at 350 and 400 °C but was transformed to Ni and MoO_2 around 500 °C. No water–gas shift catalytic activity was observed around 350 and 400 °C, but the catalytic activity rose as the concentration of Ni and MoO_2 increased at 500 °C [10]. Fig. 3(b) displays the water–gas shift catalytic activity for the Ni/MoO_2 catalyst generated in the experiments of Fig. 3(a) (Catalyst I in our notation). Good water–gas shift catalytic activity was observed at 350, 400 and 500 °C, while the structure of the Ni/MoO_2 catalyst remained unchanged [10].

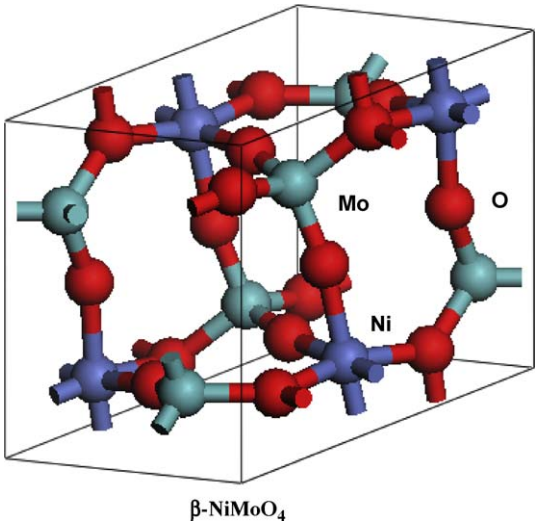

Fig. 2. Primitive cell for β-$NiMoO_4$. The red spheres represent oxygen atoms. The metal atoms are represented by light (Mo) or dark (Ni) blue spheres. (For interpretation of the references to color in this figure legend, the reader is referred to the web version of the article.)

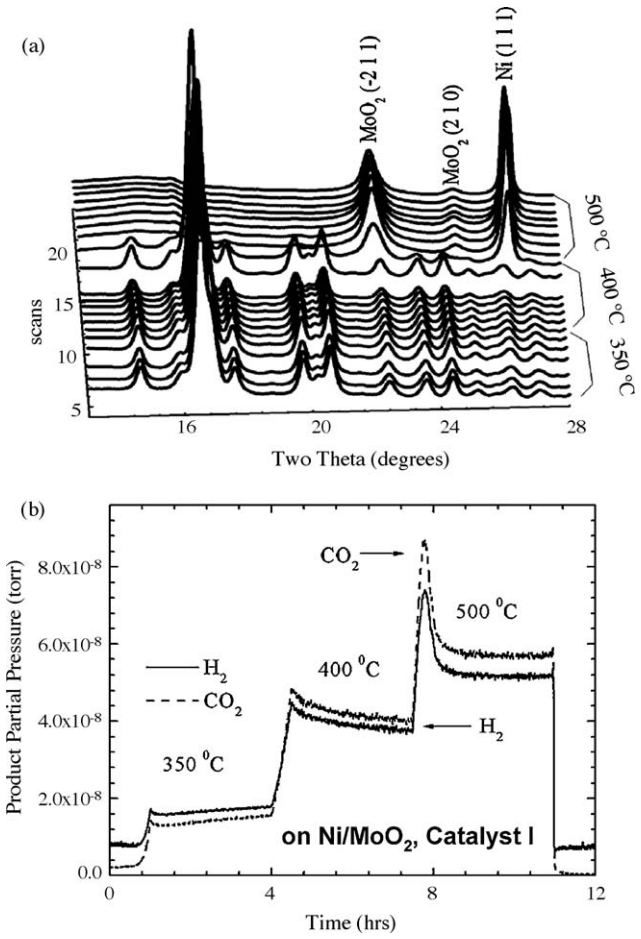

Fig. 3. (a) *In-situ* time-resolved XRD patterns collected while carrying out the water–gas shift reaction on β-$NiMoO_4$ (λ = 0.922 Å). At 500 °C, Ni/MoO_2 was generated. (b) Concentrations of H_2 and CO_2 measured after performing the WGS reaction on the Ni/MoO_2 system (i.e. Catalyst I in our notation) generated in the experiments of part (a). The water–gas shift reaction was carried out isothermally at 350, 400 and 500 °C.

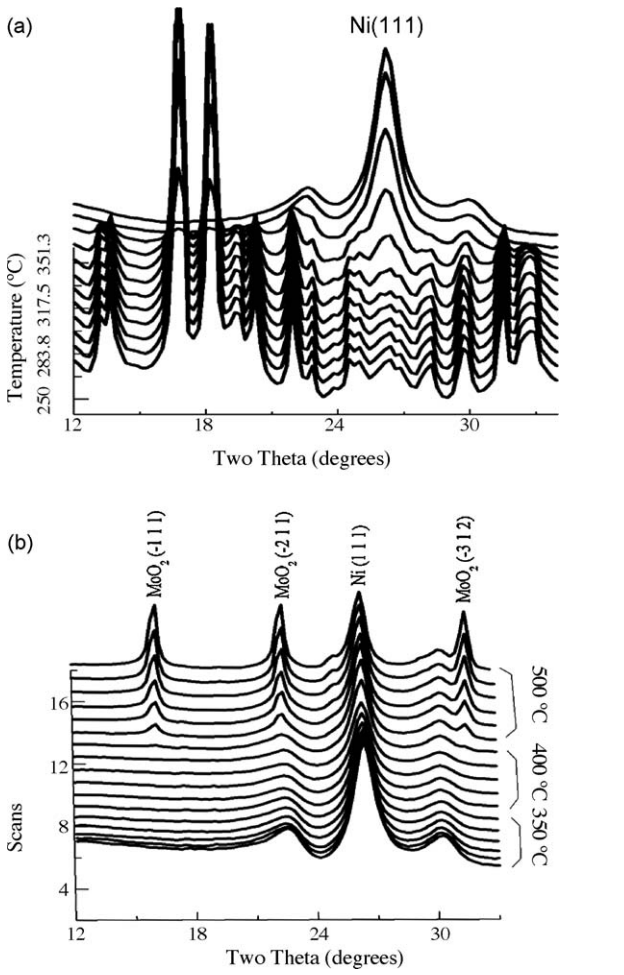

Fig. 4. (a) *In-situ* time-resolved XRD patterns, λ = 0.922 Å, collected during the reduction of a nickel molybdate in hydrogen. The temperature was ramped to 360 °C (3.75 °C/min). (b) *In-situ* time-resolved XRD patterns, λ = 0.922 Å, collected after exposing the Ni/MoO_x system prepared in part (a) to the reactants for the WGS. The WGS reaction was carried out isothermally at 350, 400 and 500 °C. This led to the generation of Catalyst II in our notation.

Looking at the β-$NiMoO_4$ → Ni-MoO_2 transformation in Fig. 3, one can wonder what induces this reduction process and if H_2 or CO could be used to pre-activate the mixed-metal oxide. The top of Fig. 4 displays *in-situ* XRD patterns collected during reduction with pure hydrogen of a nickel molybdate. At 350 °C, the diffraction peaks of the mixed-metal oxide disappeared and those of metallic Ni increased gradually. The reduced system consisted of a mixture of amorphous molybdenum oxide and metallic Ni [10]. The bottom of Fig. 4 shows diffraction patterns collected after exposing the reduced nickel molybdate to the reactants of the water–gas shift at 350, 400 and 500 °C. The material remains unchanged at 350 and 400 °C, while a gradual crystallization of MoO_2 was observed around 500 °C. The final product consisted of a mixture of Ni and MoO_2, Catalysts II in our notation, which was very active for catalyzing the water–gas shift [10].

A Rietveld analysis of the XRD data for Catalyst II gave a Ni phase refined to a space group of *fm3m* symmetry with lattice parameters of $a = b = c = 3.529$ Å [10]. The MoO_2 was refined to a space group of $P2_1/c$ symmetry with lattice parameters of $a = 5.632$ Å, $b = 4.865$ Å and $c = 5.564$ Å [10]. In Catalyst II the intensity of the $MoO_2(-1\ 1\ 1)$ diffraction peak (around the two-theta angle of 15°) is weaker than expected if compared with standard MoO_2 [18]. In addition, the Rietveld refinement of the XRD pattern for Catalyst II points to a Ni/MoO_2 ratio of 1/0.36, which is much larger than the ratio 1 expected after using a $NiMoO_4$ precursor. Thus, a very large fraction of the MoO_x present in Catalyst II is amorphous or has short range order [10]. Measurements of X-ray absorption spectroscopy at the Mo L_{III}-edge indicated that MoO_2 was the dominant molybdenum oxide present in Catalysts II [10].

The XRD patterns of MoO_2, Catalyst I, and Catalyst II are compared in the top panel of Fig. 5 [10]. Since MoO_2 is not stable under ambient conditions and usually forms a thin layer of MoO_3, the XRD pattern of MoO_2 was obtained *in-situ* after two passes of the water gas shift reaction. As in the case of Catalyst II, Catalyst I contains only Ni and MoO_2. For catalyst I the peak intensity of the MoO_2 $(-1\ 1\ 1)$ diffraction is even smaller than in Catalyst II and the diffraction lines of nickel clearly dominate the XRD pattern. The variations in the intensity of the MoO_2 $(-1\ 1\ 1)$ diffraction in catalysts I and II could be due to the effect of a substantial concentration of O vacancies which may lead to the formation of "stacking faults" and a systematic extinction of certain diffraction peaks [10]. We saw uniform diffraction rings, which is not consistent with a preferred orientation of the powder sample. A width analysis of the diffraction peaks using the Scherrer's equation indicated that size of the MoO_2 particles was comparable for Catalysts I (~13 nm) and II (~16 nm), while the Ni particle size in Catalyst II (~7.5 nm) was substantially smaller than in Catalyst I

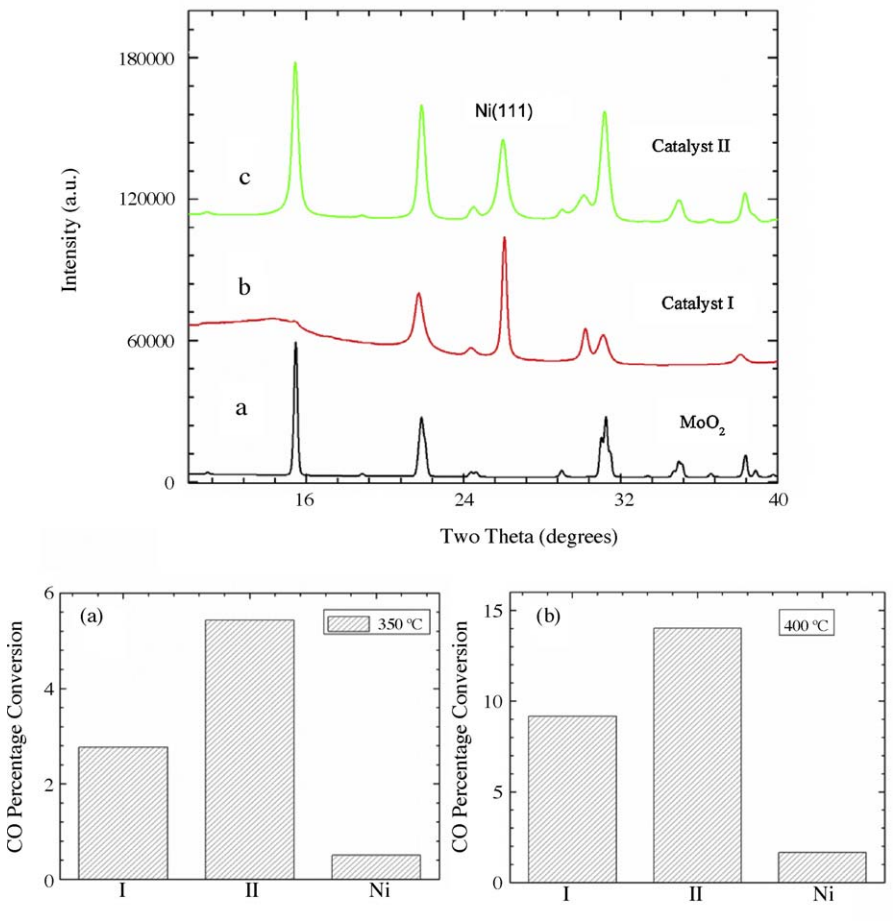

Fig. 5. Top panel: XRD patterns for Catalyst I, Catalyst II and MoO_2 (λ = 0.922 Å). Bottom panels: percentage of CO conversion during the water–gas shift reaction over Catalyst I, Catalyst II and Ni. The CO percentage conversion was averaged over a period of 3 h for each temperature (350 or 400 °C).

(~29 nm) or the Ni powder (~33 nm). This difference in Ni particle size was confirmed by images of transmission electron microscopy (TEM).

The CO percentage conversion for catalysts I, II and a Ni powder during the WGS reaction is displayed in the bottom panels of Fig. 5. Among these systems, Catalyst II displays the highest activity at both 350 and 400 °C. Catalyst I has a more significant CO conversion capability than the Ni powder. At 350 and 400 °C, we found that MoO_2 did not display any WGS activity [9,10], which indicates a cooperative interaction between the nickel clusters and the molybdenum oxide support. According to the XRD results, Catalyst II exhibits the bigger MoO_2 (−1 1 1)/MoO_2 (−2 1 1) intensity ratio, the smallest Ni particle size, and the highest WGS activity [10].

In a separate set of experiments, we investigated the WGS reaction over $CuMoO_4$ finding a very small catalytic activity [9]. During the water–gas shift reaction, the $CuMoO_4$ transformed to three different phases. Around 320 °C, an intermediate phase, which could not be identified, was formed. Next, $Cu_{4-x}Mo_3O_{12}$ was observed at 350 °C. At higher temperature, the catalyst transformed to $Cu_6Mo_5O_{18}$ and remained unchanged up to 500 °C. It was noted that the nominal oxidation state of the Mo ions decreased systematically from +6 ($CuMoO_4$) to +4.8 ($Cu_6Mo_5O_{18}$), which suggested that the gas mixture of CO and H_2O reduced the oxide matrix gradually [9].

A novel and active Cu/MoO_2 catalyst was synthesized by partial reduction of the $CuMoO_4$ precursor with CO or H_2 at 200–250 °C [9]. During the reduction process the diffraction pattern of the $CuMoO_4$ collapsed and the copper metal lines were observed on an amorphous material background that was assigned to molybdenum oxides. The first pass of the WGS led to diffraction lines for $Cu_6Mo_5O_{18}$ and MoO_2 around 350 °C and $Cu_6Mo_5O_{18}$ was further transformed to Cu/MoO_2 at higher temperature. Then, significant WGS catalytic activity was observed with relatively stable plateaus in product formation around 350, 400 and 500 °C [9]. Cu/MoO_2 was found to be more active than commercial Cu/ZnO catalysts, but not as active as Ni/MoO_2 [9,10].

3.2. Water–gas shift reaction on $Ce_{1-x}Cu_xO_{2-\delta}$ and CuO/CeO_2

CeO_2-based catalysts have been reported to be very promising for the WGS reaction owing to the peculiar redox properties of ceria and its oxygen storage capacity [19]. It is anticipated that, with proper development, CuO-CeO_2 catalysts should realize much higher CO conversions in the WGS than commercial Cu/ZnO catalysts which contain equivalent amounts of copper per unit area [19,20]. The roles played by the ceria and copper in the WGS over CuO-CeO_2 catalysts are a matter of debate [21]. Either metallic Cu or Cu^{1+} cations have been proposed as active sites for the WGS reaction. On the other hand, ceria may not be a simple spectator and play a direct role in the catalytic process [19,20]. In a recent study, *in-situ* time-resolved XRD was employed to examine the behavior of CuO_x/CeO_2 and $Ce_{1-x}Cu_xO_{2-\delta}$ nanoparticles under different WGS reaction conditions and gas environments [11]. Pure CeO_2 adopts a fluorite structure in which the metal cations are in a structural configuration quite different from that found in Cu_2O or

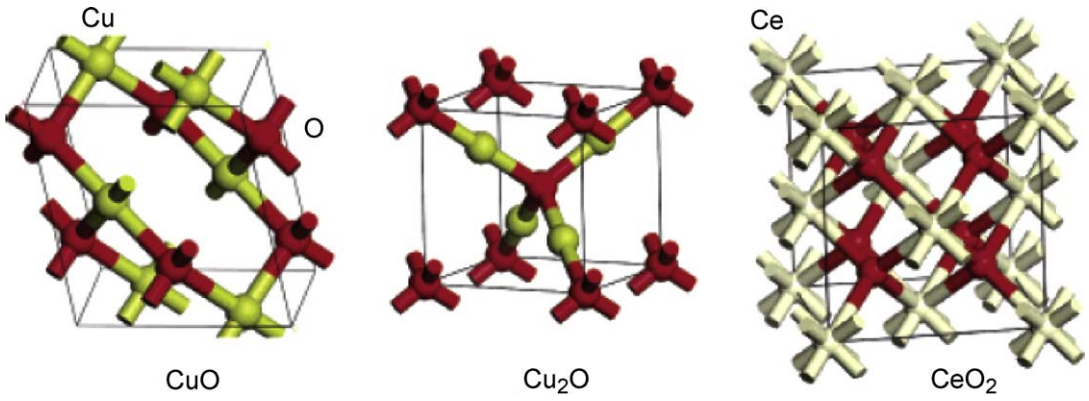

Fig. 6. Crystal structures for CuO, Cu_2O and CeO_2.

CuO, see Fig. 6. Mixed-metal oxides of the $Ce_{1-x}Cu_xO_{2-\delta}$ type can be prepared, but the Cu cations inside the ceria lattice exhibit big structural and electronic perturbations with respect to the cations in Cu_2O or CuO [22].

A typical set of time-resolved XRD patterns is shown in Fig. 7 for a $Ce_{0.8}Cu_{0.2}O_{2-\delta}$ catalyst exposed to a mixture of CO and H_2O at different temperatures [11]. No copper or copper oxides were observed at low temperatures (<100 °C) when only the diffraction lines of pure ceria are seen. It must be taken into account in this respect that under these conditions the Cu atoms are more or less uniformly distributed through the bulk and the surface of the ceria particles [11,22]. However, clear features for metallic copper were seen at temperatures of 150 °C or above. This reveals that copper sinters during reduction under WGS conditions in this sample, as shown to occur also under H_2 [22]. The mass spectrometer signals for H_2 and CO_2 in Fig. 7(b) show a low WGS activity at temperatures below 200 °C, and much higher activity at 300 and 400 °C with the presence of metallic copper. Very similar results were found when examining the behavior of $Ce_{0.95}Cu_{0.05}O_{2-\delta}$ and CuO/CeO_2 catalysts [11]. The *in-situ* XRD results show the important role of metallic copper in the WGS.

Measurements of X-ray absorption spectroscopy at the Ce L_3-edge indicate that O vacancies are formed in the ceria lattice during the WGS [11]. Since Ce^{3+} is bigger with respect to Ce^{4+}, a simple reduction leads to a ceria lattice cell expansion [11,22]. Changes in the ceria lattice parameter can be directly related to the concentration of oxygen vacancies or Ce^{3+} cations in the oxide. Fig. 8(a) shows the lattice parameter for ceria determined from (1 1 1) diffraction peaks of time-resolved XRD patterns for $Cu_{0.2}Ce_{0.8}O_{2-\delta}$ under different gases at 400 °C. The sample was first heated to 400 °C in He. The ceria lattice constant displayed a significant increase after exposure to CO and a decrease in H_2O, indicating that CO reduced ceria while H_2O oxidized it. In other words, CO created oxygen vacancies ($CO + O_{oxi} \rightarrow CO_2 + O_{vac}$) while H_2O eliminated them ($H_2O + O_{vac} \rightarrow O_{oxi} + H_2$). In the bottom panel of Fig. 8 are summarized the results of gas-switch experiments for $Cu_{0.2}Ce_{0.8}O_{2-\delta}$ at different temperatures. The ceria lattice parameter under the WGS reaction reflects a combination of the effects of CO reduction and H_2O oxidation, implying that oxygen vacancies on the fluorite phase are involved in the chemistry of the process [11].

3.3. Water–gas shift reaction on $CuFe_2O_4$

In this section, we present our new results examining the structural behavior of $CuFe_2O_4$ under WGS reaction conditions. Our interest in this compound is due to the fact that Cu–Fe oxides are used as WGS catalysts in some industrial processes [12]. The structure of $CuFe_2O_4$, known as an "inverse spinel", contains both octahedral and tetrahedral cation sites (see Fig. 9) [23,24]. Copper ions sit predominantly on octahedral sites and iron atoms split between the two [24]. $CuFe_2O_4$ is cubic at elevated temperatures (>400 °C) and tetragonal with the axial ratio $c/a > 1$ at room temperature [23].

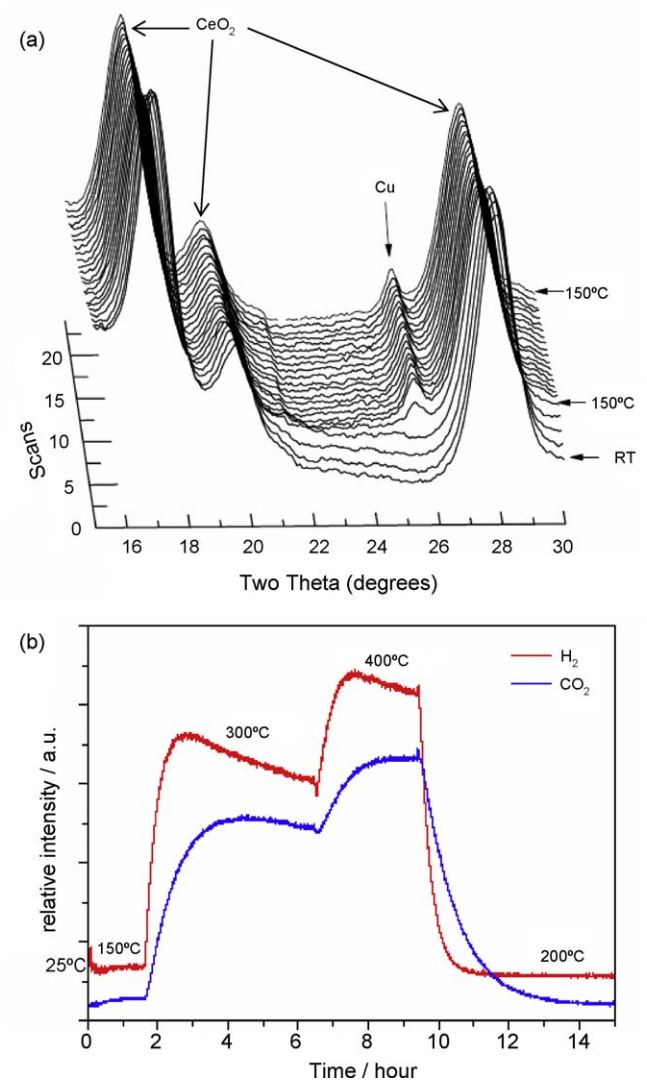

Fig. 7. Top: time-resolved XRD diffraction patterns for $Ce_{0.8}Cu_{0.2}O_{2-\delta}$ during the WGS reaction at different temperatures (λ = 0.922 Å). Bottom: the relative concentration of H_2 and CO_2 products as a function of time at different temperatures during the WGS. The WGS reaction was carried out isothermally at 150, 300 and 400 °C, with a flow of 5% CO/95% He gas through a water bubbler at a rate of ~10 ml/min.

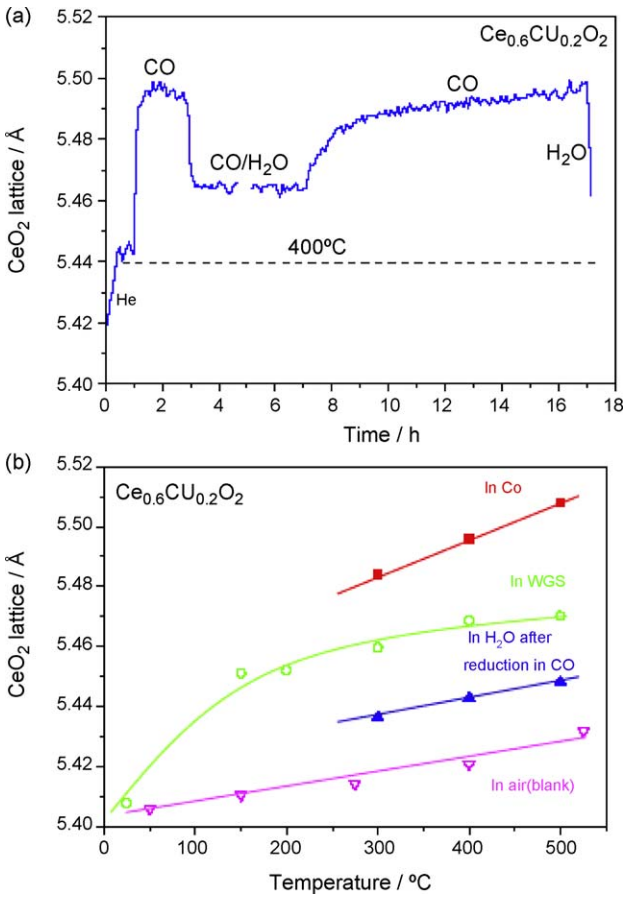

Fig. 8. (a) Ceria lattice parameters during gas-switch experiments over a $Ce_{0.8}Cu_{0.2}O_{2-\delta}$ catalyst at 400 °C. (b) Ceria lattice parameters of $Ce_{0.8}Cu_{0.2}O_{2-\delta}$ in the gas-switch experiments as a function of temperature.

Fig. 10 shows a series of XRD patterns collected during the heating of $CuFe_2O_4$. As the temperature was raised, the diffraction lines for the tetragonal phase disappeared at ~380 °C leaving only diffraction lines for the cubic phase. This is in agreement with previous studies of X-ray diffraction for the mixed-metal oxide

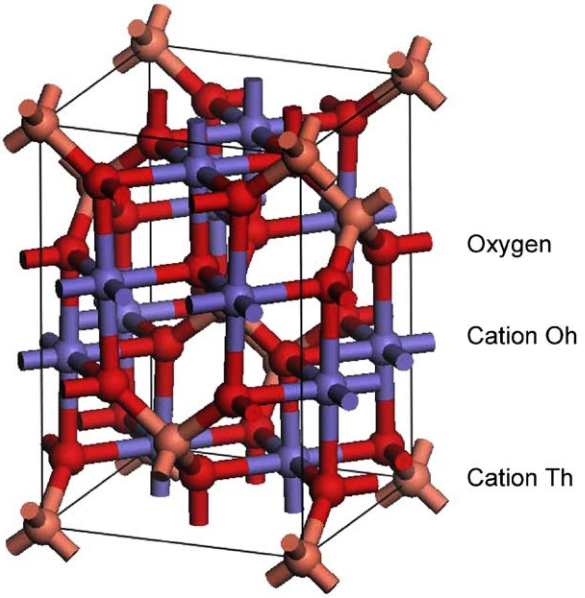

Fig. 9. Crystal structure for $CuFe_2O_4$.

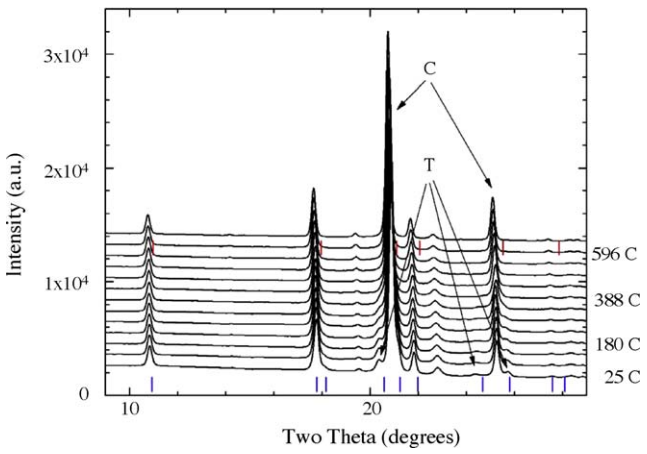

Fig. 10. XRD patters collected during the heating of $CuFe_2O_4$ in air (λ = 0.922 Å). T and C refer to diffraction lines for the tetragonal and cubic phases, respectively.

[23]. We found that the onset for WGS activity on $CuFe_2O_4$ occurred at a lower temperature than the tetragonal → cubic phase transition. In fact, before the phase transition occurs, the tetragonal structure reacts with CO or H_2 around 200 °C, undergoing partial reduction to yield metallic Cu, $CuFe_5O_8$ or Fe_3O_4. $CuFe_5O_8$ and Fe_3O_4 have both a spinel structure and are very difficult to distinguish by XRD diffraction.

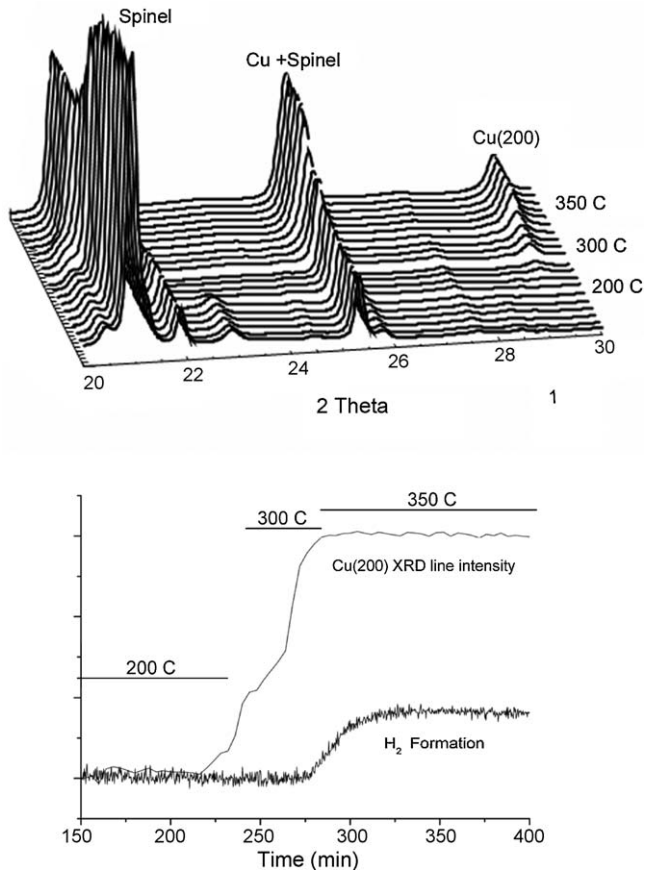

Fig. 11. Top: time-resolved X-ray diffraction patterns for a $CuFe_2O_4$ catalyst during the water gas shift reaction at different temperatures (λ = 0.922 Å). The label "spinel" is used to denote $CuFe_5O_8$ and/or Fe_3O_4. Bottom: segregation of copper and H_2 formation as a function of time and temperature. The WGS reaction was carried out isothermally at 200, 300 and 350 °C.

Fig. 11 displays XRD data collected while performing the WGS on $CuFe_2O_4$ at different temperatures. Up to ~200 °C, there were no changes in the tetragonal structure of $CuFe_2O_4$ and no WGS activity was detected. From 200 to 300 °C, the CO attacks the oxide and partial reduction leads to the segregation of metallic Cu with the onset of WGS activity. At 350 °C, one has an active WGS catalysts which contains a mixture of Cu, $CuFe_5O_8$ and/or Fe_3O_4. The intensity of the Cu (2 0 0) diffraction line becomes constant and Scherrer's analysis of its width gave a Cu particle size of ~23 nm. A Rietveld refinement gave a mole ratio of ~1 for the diffraction lines of Cu and the $CuFe_5O_8/Fe_3O_4$ spinel. *In-situ* experiments of X-ray absorption spectroscopy at the Cu K-edge indicated that essentially all the Cu^{2+} initially present in $CuFe_2O_4$ had been reduced to metallic Cu^0. These XRD results point to metallic copper as an active species for the WGS. In this respect, all the *in-situ* XRD measurements described in this article agree with similar studies previously done for CuO–ZnO [3]. The Cu^{2+} cations located inside the lattices of the mixed-metal oxides are not stable under the reaction conditions of the WGS. The thesis that metallic copper is an essential component in the active phase of WGS catalysts is also supported by kinetic data which show that extended surfaces of copper [25–27] and copper nanoparticles supported on metal-oxides [13,27,28] are active catalysts for the WGS. In Cu/oxide WGS catalysts, the main role of the oxide probably involves the dissociation of water [13,27,28], while other steps of the reaction can take place on the metal or metal–oxide interface [21,33]. Oxides like MoO_2, CeO_2 and Fe_3O_4 are better as supports than oxides such as ZnO, MgO and Al_2O_3, because the first ones contain cations which can switch oxidation states, depending on the content of O vacancies, and are more efficient for the dissociation of the O–H bonds in water [13,27,28].

4. Conclusion

The results described above show how powerful can be time-resolved XRD for studying the behavior of heterogeneous catalysts *in-situ* during reaction conditions. The examples discussed are for mixed-metal oxide catalysts, but the technique has also been applied successfully to study fluoride, sulfide, carbide and phosphide catalysts [4–8,13,29–32]. Time-resolved XRD can identify the active phase of a heterogeneous catalyst and how its structure changes after interacting with the reactants and products.

Under WGS reaction conditions, mixed-metal oxides such as $CuMoO_4$, $NiMoO_4$, $Ce_{1-x}Cu_xO_{2-\delta}$ and $CuFe_2O_4$ undergo partial reduction. The data of time-resolved XRD indicate that metallic copper or nickel and oxygen vacancies in the oxide component are involved in the generation of active sites for the production of hydrogen through the water–gas shift reaction. In the case of $Ce_{1-x}Cu_xO_{2-\delta}$, Rietveld refinement shows expansions/contractions in the oxide lattice which track steps within the WGS process: $CO(gas) + O(oxi) \rightarrow CO_2(gas) + O\ (vac)$; $H_2O(gas) + O(vac) \rightarrow O(oxi) + H_2(gas)$.

Acknowledgement

The work at BNL was financed by the US Department of Energy (DOE), Chemical Sciences Division (DE-AC02-98CH10086). The National Synchrotron Light Source is supported by the Divisions of Materials and Chemical Sciences of US-DOE. FONICIT financed the work at IVIC (G-2000001547 and G-2005000444).

References

[1] P. Norby, J.C. Hanson, Catal. Today 39 (1998) 301.
[2] J.M. Thomas, G.N. Greaves, Science 265 (1994) 1675.
[3] B.S. Clausen, G. Steffensen, B. Fabius, J. Villadsen, R. Feidenhansl, H. Topsoe, J. Catal. 132 (1991) 524.
[4] J.A. Rodriguez, S. Chaturvedi, J.C. Hanson, J.L. Brito, J. Phys. Chem. B 103 (1999) 770.
[5] J.A. Rodriguez, J.C. Hanson, S. Chaturvedi, A. Maiti, J.L. Brito, J. Chem. Phys. 112 (2000) 935.
[6] J.A. Rodriguez, J.C. Hanson, S. Chaturvedi, A. Maiti, J.L. Brito, J. Phys. Chem. B 104 (2000) 8145.
[7] P. Norby, F.I. Poshni, A.F. Gualtieri, J.C. Hanson, C.P. Grey, J. Phys. Chem. B 102 (1998) 839.
[8] P. Norby, J. Am. Chem. Soc. 119 (1997) 5215.
[9] W. Wen, L. Jing, M.G. White, N. Marinkovic, J.C. Hanson, J.A. Rodriguez, Catal. Lett. 113 (2007) 1.
[10] W. Wen, J.E. Calderon, J.L. Brito, N. Marinkovic, J.C. Hanson, J.A. Rodriguez, J. Phys. Chem. C 112 (2008) 2121.
[11] X. Wang, J.A. Rodriguez, J.C. Hanson, D. Gamarra, A. Martinez-Arias, M. Fernandez-Garcia, J. Phys. Chem. B 110 (2006) 428.
[12] D.S. Newsome, Catal. Rev. Sci. Eng. 21 (1980) 275.
[13] J.A. Rodriguez, P. Liu, J. Hrbek, M. Pérez, J. Evans, J. Mol. Catal. A 281 (2008) 59.
[14] P.J. Chupas, M.F. Ciraolo, J.C. Hanson, C.P. Grey, J. Am. Chem. Soc. 123 (2001) 1694.
[15] P. Chupas, K. Chapman, C. Kurtz, J. Hanson, P. Lee, C.P. Grey, J. Appl. Cryst. 41 (2008) 822.
[16] A.P. Hammersley, S.O. Svensson, A. Thompson, Nucl. Instrum. Methods Phys. Res. Sect. A 346 (1994) 312.
[17] (a) A.C. Larson, R.B. von Dreele, GSAS General Structure Analysis System. Report LAUR 86-748, Los Alamos National Laboratory: Los Alamos, NM, 1995.
(b) H.M. Reitveld, J. Appl. Cryst. 2 (1969) 65;
(c) B.H. Toby, J. Appl. Cryst. 34 (2001) 210.
[18] Natl. Bur. Stand. (U.S.) Monogr. 25, 18, 44, (1981).
[19] Y. Li, Q. Fu, M. Flytzani-Stephanopoulos, Appl. Catal. B 27 (2000) 179.
[20] Y. Liu, T. Hayakawa, K. Suzuki, S. Hamakawa, Catal. Commun. 2 (2001) 195.
[21] T. Bunluesin, R. Gorte, G. Graham, Appl. Catal. B 15 (1998) 107.
[22] X. Wang, J.A. Rodriguez, J.C. Hanson, D. Gamarra, A. Martinez-Arias, M. Fernandez-Garcia, J. Phys. Chem. B 109 (2005) 19595.
[23] H. Ohnishi, T. Teranishi, J. Phys. Soc. Jpn. 16 (1961) 35.
[24] J.M. Tranquada, S.M. Heald, A.R. Moodenbaugh, Phys. Rev. B 36 (1987) 5263.
[25] J.A. Rodriguez, D.W. Goodman, Surf. Sci. Rep. 14 (1991) 1.
[26] J. Nakamura, J.M. Campbell, C.T. Campbell, J. Chem. Soc. Faraday Trans. 86 (1990 2725);
C.T. Campbell, B. Koel, Surf. Sci. 186 (1987) 393.
[27] J.A. Rodriguez, P. Liu, J. Hrbek, J. Evans, M. Perez, Angew. Chem. Int. Ed. 46 (2007) 1329.
[28] J.A. Rodriguez, P. Liu, X. Wang, W. Wen, J. Hanson, J. Hrbek, M. Pérez, J. Evans, Catal. Today, in press.
[29] J.A. Rodriguez, J.C. Hanson, A.I. Frenkel, J.Y. Kim, M. Perez, J. Am. Chem. Soc. 124 (2002) 346.
[30] J.A. Rodriguez, J.-Y. Kim, J.C. Hanson, S.J. Sawhill, M.E. Bussell, J. Phys. Chem. B 107 (2003) 6276.
[31] J.A. Rodriguez, X. Wang, G. Liu, J.C. Hanson, J. Hrbek, C.H.F. Peden, A. Iglesias-Juez, M. Fernandez-Garcia, J. Mol. Catal. A: Chem. 228 (2005) 11.
[32] J.A. Rodriguez, J.Y. Kim, J.C. Hanson, J.L. Brito, Catal. Lett. 82 (2002) 103.
[33] R. Burch, Phys. Chem. Chem. Phys. 8 (2006) 5483.